instruments

MDPI

Article

From Lab to Launchpad: A Modular Transport Incubator for Controlled Thermal and Power Conditions of Spaceflight Payloads

Sebastian Feles *, Ilse Marie Holbeck and Jens Hauslage

Aeromedical FabLab, Institute of Aerospace Medicine, German Aerospace Center (DLR), 51147 Cologne, Germany; ilsemarie.holbeck@dlr.de (I.M.H.); jens.hauslage@dlr.de (J.H.)
* Correspondence: sebastian.feles@dlr.de

Abstract

Maintaining physiologically controlled conditions during the transport of biological experiments remains a long-standing but under-addressed challenge in spaceflight operations. Pre-launch thermal or mechanical stress induce artefacts that compromise the interpretation of biological responses to space conditions. Existing transport systems are limited to basic heating of small sample containers and lack the capability to power and protect full experimental hardware during mission-critical phases. A modular transport incubator was developed and validated that combines active thermal regulation, battery-buffered power management, and mechanical protection in a compact, field-deployable platform. It enables autonomous environmental conditioning of complex biological payloads and continuous operation of integrated scientific instruments during ground-based transport and recovery. Validation included controlled experiments under sub-zero ambient temperatures, demonstrating rapid warm-up, stable thermal regulation, and uninterrupted autonomous performance. A steady-state finite difference thermal model was experimentally validated across 21 boundary conditions, enabling predictive power requirement estimation for mission planning. Field deployments during multiple MAPHEUS® sounding rocket campaigns confirmed functional robustness under wind, snow, and airborne recovery scenarios. The system closes a critical infrastructure gap in spaceflight logistics. Its validated performance, modular architecture, and proven operational readiness establish it as an enabling platform for standardized, reproducible ground handling of biological payloads and experiment hardware.

Keywords: transport incubator; spaceflight hardware; sounding rocket; microgravity research; biological payloads; thermal regulation; environmental control; battery-buffered power supply

Academic Editor: Antonio Ereditato

Received: 5 August 2025
Revised: 3 September 2025
Accepted: 15 September 2025
Published: 18 September 2025

Citation: Feles, S.; Holbeck, I.M.; Hauslage, J. From Lab to Launchpad: A Modular Transport Incubator for Controlled Thermal and Power Conditions of Spaceflight Payloads. *Instruments* **2025**, *9*, 21. https://doi.org/10.3390/instruments9030021

1. Introduction

Ensuring uninterrupted physiological conditions during the transport of biological samples is a long-standing but often neglected challenge in spaceflight research. In life science missions, the scientific objective is to isolate the effects of space conditions—such as microgravity or ionizing radiation—on biological systems. However, if biological payloads are exposed to thermal or mechanical stress before launch—during ground handling or transport—these stressors may already trigger physiological responses. As a result, subsequent observations can no longer be clearly attributed to the intended exposure in

space, compromising scientific interpretability. Despite the well-known susceptibility of sensitive payloads to such artefacts, technical infrastructure for controlled, flight-relevant transport has lagged behind. This gap limits the reproducibility and validity of spaceflight experiments and calls for a robust enabling platform to ensure stable conditions throughout all mission phases.

These limitations become particularly evident when considering the operational context and environmental challenges of modern spaceflight platforms. Platforms such as drop towers, human centrifuges, parabolic flight planes and suborbital flights require specialized systems to maintain physiological conditions throughout sample preparation, transfer, and launch operations [1]. In particular, sounding rocket campaigns pose substantial technical and logistical constraints [2].

In Europe, these campaigns are typically conducted at remote, high-latitude sites such as the European Space and Sounding Rocket Range (ESRANGE) in Kiruna, Sweden, or Andøya Space Center in Norway. While launch infrastructure also exists in other regions, these locations dominate biological mission planning due to their technical capabilities and range access [3,4].

Transport to the launch pad is complicated by frequent weather-related delays, including rapid temperature drops and strong winds, with ambient temperatures occasionally falling below -40 °C. Samples must be kept within strict physiological limits to avoid degradation and experimental artefacts [5]. Additionally, low humidity increases the risk of electrostatic discharge (ESD), affecting sensitive electronics [6].

The complexity of modern biological payloads further amplifies the need for transport stability. Many biological systems are acutely sensitive to short-term environmental deviations that affect metabolism, enzyme activity, or gene expression [7,8]. These challenges are particularly evident in experiments involving neuronal cell lines, primary cultures, or genetically encoded reporters [9–11]. Without adequate thermal regulation, low temperatures impair proliferation and protein biosynthesis, while excessive heat can trigger membrane destabilization or apoptosis [12,13]. Even short-term deviations may compromise sample integrity and limit reproducibility.

To address this need, we have developed a transport incubator that is both modular and field-deployable (Figure 1A,B). It provides active thermal control, continuous power supply with seamless switching between battery and mains operation, and mechanical protection during all phases of sample transport. The system maintains biologically relevant temperature setpoints independently of external conditions and supports autonomous payload operation across varying environmental and power scenarios. Its robust design enables technical pre-launch checks of payload hardware and environmental conditions, environmental conditioning, and full mission readiness without depleting onboard resources. As a validated and adaptable enabling platform, it supports standardized pre-launch logistics and contributes to reproducibility and technical reliability in biological spaceflight experiments.

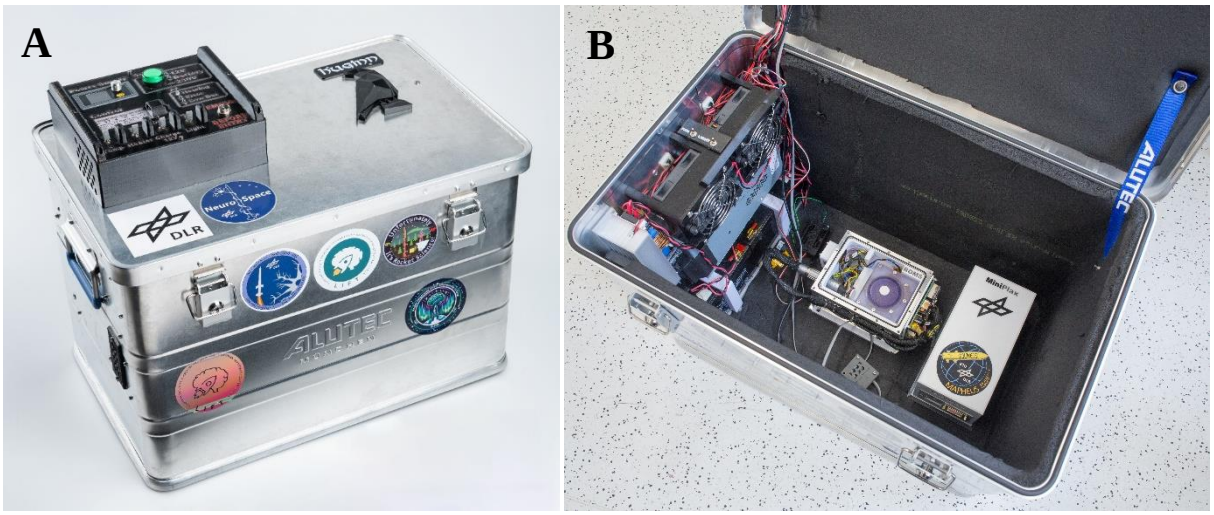

Figure 1. The transport incubator in its operational configuration. The image shows the fully assembled system including the insulated aluminium housing, control interface, and power connectors (**A**). The incubator is designed for autonomous operation under extreme environmental conditions and enables active thermal regulation and continuous power supply. The interior accommodates several experiments at once (**B**).

2. Hardware Description

The transport incubator is designed with three key objectives in mind: providing mechanical protection for experimental hardware, ensuring precise thermal regulation for both the contained hardware and biological samples, and ensuring reliable operation with a continuous power supply. Beyond these immediate technical goals, the system was deliberately conceived as a modular enabling platform—supporting diverse payload types, mission profiles, and environmental conditions. The modular and insulated incubator is designed for performance in ambient temperature ranges from -40 °C to 35 °C, ensuring stable internal conditions throughout transport, regardless of external factors. Hence, it proves especially suitable for sounding rocket campaigns, where ambient temperatures and environmental conditions can vary in a wide range.

The incubator is built from an aluminium crate, selected for its mechanical robustness and favorable strength-to-weight ratio. The external dimensions of the incubator are $575 \times 385 \times 375$ mm ^{3}, with internal dimensions of $550 \times 350 \times 355$ mm^3, providing a usable internal volume of 46 L. This size accommodates a wide range of experimental hardware configurations, e.g., 1U and 2U units, leaving sufficient space for thermal regulation and power management systems.

To enhance durability, the crate is reinforced along the edges and corners, enabling it to withstand the environmental and mechanical challenges of aerial recovery operations. Following parachute descent and touchdown in remote terrain, the payload is typically retrieved under cold and snowy conditions, often requiring helicopter transport through difficult landscapes (Figure 2A). The incubator maintains internal thermal stability throughout this process, protecting temperature-sensitive samples from sub-zero exposure. Since external handling is performed with care and without significant impact loading, no dedicated internal damping system was required, as the closed-cell elastomeric insulation already provides sufficient passive vibration attenuation. Minor mechanical stresses and transport-induced vibrations—such as those encountered during helicopter or ground vehicle transport—are thereby adequately damped. The closed-cell foam structure provides damping in the low-frequency range [14]. This is particularly relevant given that structural vibration spectra in helicopters and terrestrial vehicles typically range between

5 Hz and 250 Hz [15,16], which overlaps with the biologically sensitive range: mechanical vibrations up to 200 Hz are known to influence cellular proliferation, differentiation, and gene expression [17,18]. The combination of passive damping and reinforced crate design therefore contributes to maintaining the mechanical and biological integrity of experimental payloads during transport under realistic operational conditions (Figure 2B).

Figure 2. Transport incubators used to recover the rocket payload during the MAPHEUS-14 sounding rocket campaign. The incubators were delivered to the remote landing site by helicopter and subsequently transported through deep snow to retrieve and preserve the experimental modules under controlled conditions (**A**). Operation under extreme conditions in the northern Swedish tundra. After removing the experiment modules from the payload, they are recovered on-site and powered by the internal electrical system of the transport incubators. The return transport is conducted under controlled conditions within the incubators, ensuring protection during helicopter transit (**B**).

The second key feature of the incubator is its thermal insulation system, designed to maintain stable internal temperatures even when exposed to extreme environmental conditions. The incubator's internal walls are lined with a layer of 19 mm of Armaflex-AF®, a closed-cell elastomeric synthetic rubber (nitrile butadiene rubber, NBR) foam known for its excellent thermal resistance (λ = 0.033 W/(m·K)) [19]. This passive insulation significantly reduces heat exchange between the internal chamber and the external environment, lowering the thermal load on the heating system and making it more energy-efficient to maintain the target temperature. While insulation increases thermal resistance and minimizes fluctuations, the degree of thermal stability achieved is dependent on the temperature differential between the incubator's interior and its external surroundings.

The heating system consists of two 150 W Positive Temperature Coefficient (PTC) heating elements, providing a total heating capacity of 300 W. PTC heaters are self-regulating; as the internal temperature approaches the desired setpoint (SP), the resistance of the PTC elements increases, reducing current draw and preventing overheating. This feature is crucial for maintaining not only a stable, but also an energy-efficient thermal regulation, particularly during long time periods between rocket integration and launch.

In our configuration, the PTC elements operate below their characteristic plateau region (typically around 100 °C to 120 °C, depending on airflow and load), as the chamber temperature is actively regulated by the microcontroller. Forced convection and a limited control target (near physiological temperatures) ensure that the PTCs remain well below their intrinsic self-limiting threshold, which acts as a passive safety feature in case of control failure.

Air circulation within the incubator is facilitated by two axial fans, each with a flow rate of 54 m^3/h, ensuring uniform heat distribution and preventing temperature stratification. This uniformity is important for biological samples, which are often sensitive to even minor temperature fluctuations. It allows the system to maintain constant temperature within ±0.76 °C, even at physiologically relevant setpoints such as 37 °C. While a full spatial temperature mapping was not performed in this study, forced convection by two 54 m^3/h fans is used to minimize gradients in the small chamber volume. Furthermore, the fans accelerate the heating process through forced convection, enabling the incubator to reach the target temperature more quickly, even when starting from sub-zero ambient conditions. At the same time, they prevent the formation of hot or cold spots within the system.

Condensation within the transport incubators poses a potential risk, particularly when transitioning between environments with varying temperature and humidity levels. However, during winter campaigns in Sweden, where the incubators are frequently deployed, the risk of condensation is significantly mitigated by the extremely low absolute humidity [20]. In these conditions, absolute humidity frequently drops below 0.01 g/m^3, significantly reducing the potential for moisture accumulation within the incubator. To further attenuate condensation risks, dehumidifier packs containing silica gel orange beads (Carl Roth, Karlsruhe, Germany) are placed inside the incubator chamber during module transport and pre-heating. When experiment modules at room temperature (21 °C) are introduced into the preheated incubator (37 °C), silica gel desiccants help control humidity levels. By lowering relative humidity from an initial 30% to a target of 12%, the dew point remains below room temperature, effectively preventing condensation on the surfaces of the experiment modules. Based on the effective air volume within the insulated chamber, 5 g of silica gel orange beads provide sufficient adsorption capacity to maintain low humidity levels during transport. This strategy safeguards the modules from condensation and therefore from electrical short circuits.

The incubator's environmental control unit integrates the thermal regulation and power management systems. Housed in a 3D-printed casing for mechanical durability, the control unit includes recessed switches, indicator lights, and oversized control buttons, all designed for easy use in harsh environments where operators may be wearing heavy gloves. The system provides real-time feedback of the operational status of the incubator, including power source selection, heating activity, and battery charge levels, ensuring that critical environmental parameters are always monitored. Battery voltage is continuously monitored by the Arduino, with the measurement calibrated against a laboratory bench multimeter. The values are internally processed to trigger undervoltage and overvoltage warnings and are permanently displayed on the front panel. In case of external vehicle power supply, the input voltage is monitored in the same way.

The temperature setpoint is configured via a protected service menu during setup, while chamber temperature is continuously displayed on the front panel. During pre-launch handling, operators continuously monitor the front-panel temperature readout. Importantly, the rapid warm-up phase is conducted before biological payloads or experimental hardware are placed inside the incubator. In case of a transient overshoot during this phase, the chamber is briefly vented prior to loading heat-sensitive samples. In addition, the control unit features a dedicated warning lamp that clearly indicates a fault if a strong deviation from the setpoint occurs during operation.

The control system is based on an Arduino-compatible Mega Pro Embed ATMega2560 Extra Mini (EnM Industry, Aachen, Germany) microcontroller, which manages the incubator's environmental control processes. This microcontroller continuously monitors internal conditions via calibrated sensors, adjusting heating and power systems as necessary to maintain optimal conditions for the experimental hardware and biological samples. Its extended operating temperature ranges from −40 °C to 85 °C, ideally suited for these harsh environments.

Electronic System

The electronic system provides stable power to both the incubator's heating system and the experimental hardware during transportation and recovery, regardless of external power availability. The system integrates multiple power sources, redundant battery systems, and advanced power management technologies to guarantee uninterrupted functionality.

The incubator's power system is engineered for flexibility, capable of drawing energy from multiple sources, including mains electricity (230 V AC), vehicle power supplies (12–24 V DC), and an internal battery system (Figure 3). The primary power source during transportation is the internal battery system, which consists of two 50 Wh, 12 V DC gel lead-acid batteries connected in series. This configuration provides a total energy capacity of 100 Wh. Gel lead-acid batteries were chosen for their robustness, low self-discharge rates, and, most critically, their reduced risk of fire or explosion under extreme conditions, making them ideal for use in these kinds of application [21,22]. The incubator's electrical system is designed with an uninterruptible power supply (UPS) configuration, ensuring continuous operation under all circumstances. External power sources, such as mains power or vehicle voltage, are looped through the internal battery system. In the event of external power failure, the system seamlessly switches to internal battery operation without any interruption in power delivery to the incubator systems. Protective diodes are incorporated into the design to prevent back feeding, ensuring that neither the DC–DC converter nor the switching power supply can feed power back through the internal batteries. The batteries are housed within the incubator's insulated compartment to maintain a stable temperature during transport. Battery performance degrades significantly when exposed to extreme cold, with energy capacity dropping sharply as temperatures fall [23]. By keeping the batteries within the temperature-controlled environment of the incubator, their performance is stabilized, ensuring reliable power output.

When connected to a mains power supply, the internal batteries are charged through an integrated 230 V AC switching power supply. The integrated charging circuit enables full battery charging during pre-launch preparation, ensuring maximum operational endurance when external power is no longer available. For vehicle power operation, the system utilizes a buck-boost DC–DC converter, stepping up the vehicle's input voltage to a stable 28 V DC output. This allows consistent operation regardless of fluctuations in the vehicle's electrical system, such as voltage drops or surges. The power management system is also equipped with an electromagnetic interference (EMI) filter, which protects sensitive hardware from voltage spikes and electrical noise that could disrupt critical systems or data collection.

The laboratory power supply module (XYS3580) located on the central control unit regulates the output voltage and current supplied to the experimental hardware. The module provides an output voltage range and current range of 0.6–36 V DC and 0–5 A, respectively, with a maximum power output of 80 W. Voltage and current resolutions are 0.01 V and 0.001 A, respectively, with accuracy ratings of ±0.3% for voltage and ±0.4% for current. These control capabilities ensure that the experimental hardware receives a stable power supply throughout the whole transportation process, regardless of the incubator's power source.

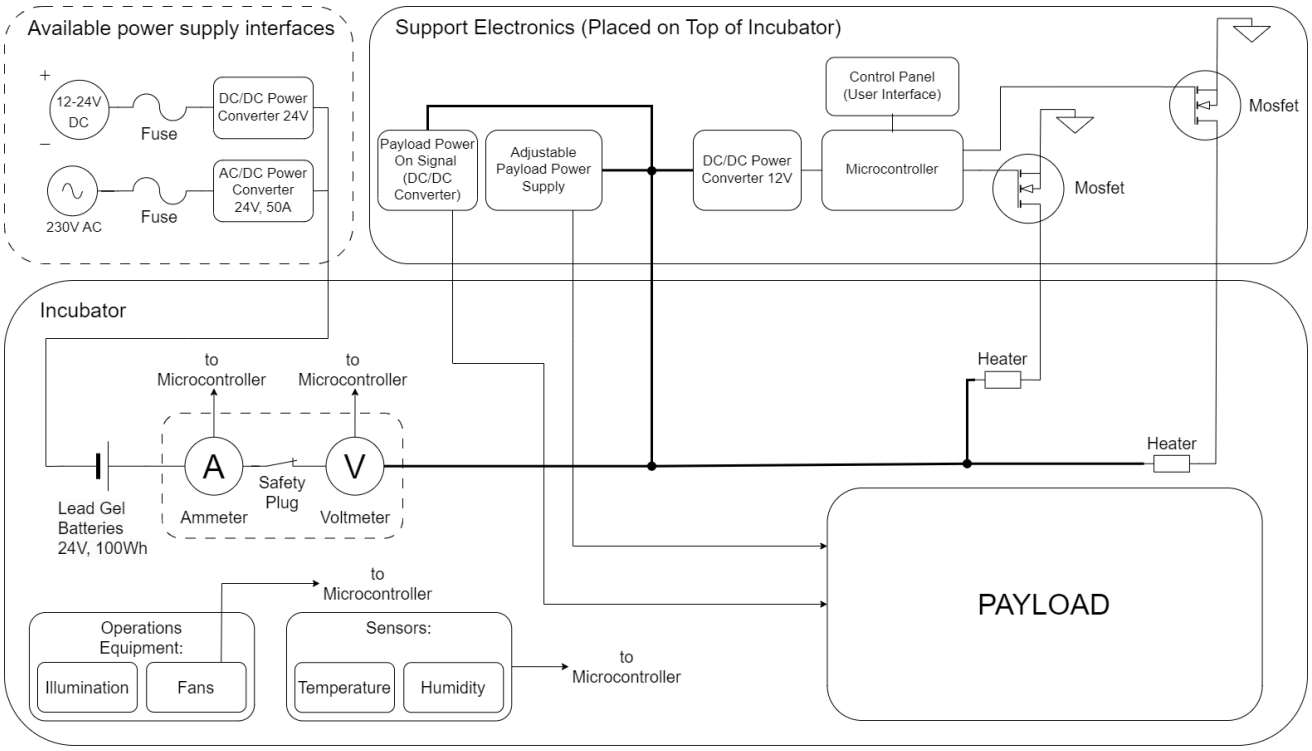

Figure 3. Simplified electrical circuit diagram of the transport incubator system, illustrating the two main components: the incubator chamber and the control unit. The diagram highlights dual power input options, including 12–24 V DC and 230 V AC mains input. The DC voltage is regulated by a buck-boost converter, while the AC input is managed by a switching power supply, providing adaptable power sources for different operational conditions. The heating system and its control circuitry within the incubator chamber ensure precise temperature regulation. An integrated programmable DC power supply provides precisely regulated voltage and current to the experimental payload.

The system also includes an LM2596S step-down DC–DC converter, which provides a constant voltage output between 1.25 V and 22 V DC at up to 2 A. This converter is used to simulate the signal normally provided by the rocket's service module, which indicates the end of the radio silence period. For our payloads, this auxiliary control voltage is identical across campaigns and is therefore configured once before deployment using a trimmer potentiometer. As this adjustment is mechanically fixed and not accessible during field operation, accidental changes are excluded.

Radio silence refers to a mandatory communication blackout during critical phases of rocket preparation, arming and during payload integration. It is enforced to prevent unintentional ignition of rocket motors, which could be triggered by electromagnetic interference, inductive transients, or other electrical disturbances. During this time, only certified passive or non-switching hardware may remain powered.

While the incubator's internal power supply keeps the experiment module's batteries charged during transport, the control electronics responsible for recording experimental data must remain off until the end of radio silence. The LM2596S provides a stable voltage signal that mimics the service module's release signal, allowing the experiment module to resume full operation—just as it would during an actual flight.

Additionally, the system can display parameters including power consumed, operating time, and the power history of the system. This information is used for monitoring energy consumption during extended campaigns, allowing operators to assess the remaining battery life and power needs for the experimental hardware. The display module consists of an illuminated e-ink display, which remains clearly legible even under challenging lighting

conditions such as direct sunlight or low-light environments. In contrast to conventional LCDs, the e-ink technology passively retains the last displayed values even in the event of a power failure—providing a persistent readout for diagnostic or documentation purposes during field operations.

For safety during radio silence and entering EMI sensitive zones at the launch site, the incubator is equipped with a clearly visible safety plug that allows for complete de-energization when necessary. The positive lead of the internal batteries is routed through this safety plug, ensuring that the system is physically disconnected when the plug is removed. This design prevents accidental power-up during sensitive operations, ensuring compliance with safety protocols and radio silence.

The incubator's heating system is controlled by a Proportional-Integral (PI) controller, which continuously adjusts the power delivered to the PTC heating elements based on real-time temperature feedback. It should be noted that the PTC elements themselves are not part of the feedback loop; their self-limiting characteristic provides an intrinsic safety margin in case of controller malfunction. The PI control algorithm (with the derivative term set to zero) dynamically modulates heating output to maintain the desired internal temperature, ensuring thermal regulation with only minor overshoot and weak oscillations, which result from the deliberately strong proportional action chosen to guarantee fast recovery in cold deployments, while avoiding conditions that could compromise the integrity of biological samples [7,12,13]. To ensure rapid responsiveness under mission conditions—such as transitioning from a warm laboratory into sub-zero ambient temperatures—the controller employs a deliberately strong proportional component. This results in a fast-reacting regulation behavior that, under some conditions, may resemble a two-point control pattern. In early heating phases, the system is programmed to operate with maximum power output, intentionally prioritizing fast thermal recovery over strict setpoint adherence. Temporary overshoot beyond the target temperature is tolerated by design, as it is operationally preferable to briefly open the incubator for manual cooling rather than endure extended waiting periods due to conservative regulation. The tuning thereby meets the operational requirement of maintaining ± 1 °C stability around the setpoint during steady-state operation. This approach has proven practical and effective in time-critical scenarios, such as those frequently encountered during sounding rocket campaigns.

The system uses two redundant temperature sensors: a Dallas DS18B20 One-Wire sensor for fast temperature acquisition with a resolution of 0.5 °C, and a Sensirion SHT21 sensor for high-precision measurements with a resolution of 0.02 °C. In addition to temperature, the SHT21 also provides relative humidity data, enabling environmental monitoring and humidity control within the incubator. The dual-sensor configuration combines the rapid response of the DS18B20 with the higher accuracy of the SHT21, allowing the control system to adapt dynamically to varying operational demands. During active heating phases or environmental transitions, the controller prioritizes the faster sensor to enable prompt thermal adjustments. In contrast, the precise SHT21 readings are used to stabilize long-term temperature control and detect subtle deviations from the setpoint. This architecture ensures both fast regulation and high accuracy, while also providing fault tolerance through sensor redundancy.

To enhance reliability, the system utilizes two different types of sensors buses (I2C and 1-Wire), providing redundancy for temperature monitoring if one of the bus systems fails in operation. This increases fault tolerance, as any failure or significant discrepancy between the sensor readings is immediately flagged and displayed on the control panel as an error. This error detection ensures higher operational safety and stability, allowing the system to quickly identify and correct potential issues, thus protecting the biological materials.

3. Application and Verification

The transport incubator was deployed in multiple high-altitude rocket campaigns, including MAPHEUS-13, -14, and -15, conducted as part of the MAPHEUS research program [24]. In all missions, the system reliably maintained defined internal environmental conditions during pre-launch, ascent, landing, and recovery phases—despite sub-zero ambient temperatures, high wind exposure, and snow-covered terrain.

During these campaigns, the incubator was used to transport a range of biological payloads, including the Biodecoder system [25], which carried primary neuronal cultures, and several configurations of the MiniFix experiment [26], involving simple multicellular animals and plant samples. To meet the specific requirements of each experiment, the incubator was configured to maintain target temperatures of 22 °C, 24 °C, or 37 °C ± 2 °C. During ground operations, the incubator transported hardware and biological samples from laboratory environments to the remote launch site, and was subsequently used during payload recovery operations, including helicopter-based retrieval in remote terrain (Figure 2A). Stable conditions were preserved throughout, protecting the samples from thermal and mechanical stress. Even at external temperatures as low as −20 °C, the system consistently maintained internal temperatures within ±2 °C of the target setpoint. The integrated laboratory power supply maintained stable operating conditions for the flight electronics and heating system during all mission phases. Following flight termination, the incubator continued autonomous operation throughout recovery in the Swedish tundra, demonstrating resilience under sub-zero temperatures and mechanical stress during helicopter transport.

To validate the incubator's performance under controlled but field-relevant conditions, a series of thermal characterization experiments was conducted. These focused on active heating performance under cold ambient conditions, thermal stability near the setpoint of 37 °C, and passive cooling behavior. Further experiments investigated how battery discharge dynamics influence the incubator's ability to maintain target temperatures during prolonged autonomous operation. These validation experiments were designed to simulate elements of the real deployment scenario: cold-start conditions, battery-limited operation, and temperature maintenance throughout transport phases involving changing ambient conditions and power supply transitions.

3.1. Thermal Regulation Under Cold Ambient Conditions

The first validation experiment investigated the incubator's thermal dynamic under simulated field conditions, designed to replicate the thermal stress encountered during transport to a remote launch site (Figure 4). For this purpose, the incubator—initially equilibrated at room temperature—was transferred outdoors, where an ambient temperature of −5 °C and a wind speed of approximately 0.5 m/s (measured using a PCE-MAM 2 anemometer) prevailed. With the system powered off and the lid open, the incubator remained outside for several hours until its internal temperature and thermal mass fully equilibrated with the ambient environment.

Following thermal equilibration, the incubator was closed, powered via a 230 V mains connection, and the internal heating system activated. For this experiment, the incubator was operated without experimental hardware to isolate the dynamic response of the system itself and avoid confounding thermal inertia. This configuration represents a conservative test scenario: in real field deployments, the experimental payload is typically prewarmed—either in a laboratory incubator or at least to room temperature—prior to installation. The active heating phase started at 23 min. From this point onward, the internal temperature followed a characteristic exponential saturation curve. The data were fitted using the following model:

$$T(t) = T_{max}\left(1 - e^{-k(t-t_0)}\right),$$

where $T(t)$ denotes the internal incubator temperature at time t, T_{max} is the asymptotically reachable maximum temperature, k is the heating rate constant [1/min], and t_0 represents the time offset marking the onset of the active heating phase. The best-fit parameters were T_{max} = 41.86 °C, k = 0.073 min^{-1}, and t_0 = 23.4 min. This model captures the system's thermal inertia and describes the gradual convergence toward a steady-state temperature. The time constant of 13.7 min (corresponding to k = 0.073 min^{-1}) quantifies the effective heating dynamics. The asymptotic approach toward 41.86 °C demonstrates the incubator's ability to overcome an ambient temperature gradient of over 40 °C and achieve stable thermal regulation under external thermal load. Since measurements were obtained from centrally suspended sensors in an unloaded chamber, the data specifically reflect the intrinsic thermal control performance of the system in the absence of additional thermal mass.

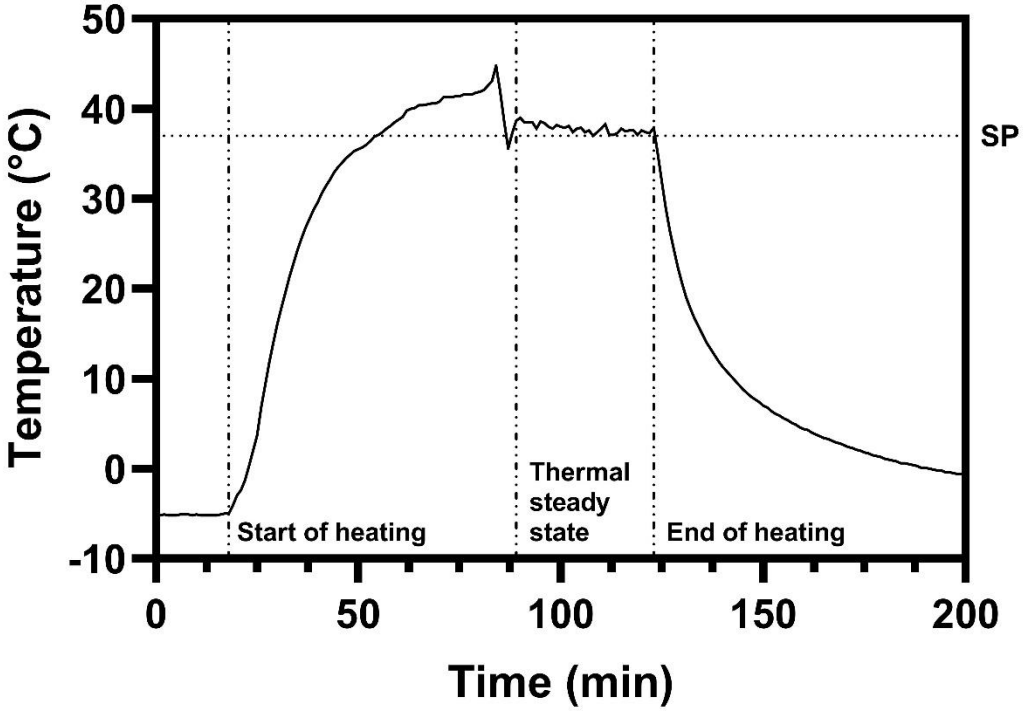

Figure 4. Internal temperature profile of the transport incubator during mains-powered operation under cold ambient conditions (–5 °C, 0.5 m/s wind). The heating phase ($t \approx$ 23–70 min) follows an exponential saturation curve as the system approaches thermal equilibrium. Between 88 and 123 min, the incubator maintains a stable internal temperature near the setpoint (SP, 37 °C) with minimal deviation with a mean of 37.81 °C and a standard deviation of 0.51 °C. After heating is manually deactivated (t > 123 min), the temperature decays exponentially.

Between 88 and 123 min, the system reached thermal steady state and maintained regulated internal conditions. During this interval, internal temperature was maintained at a mean of 37.81 °C, with a standard deviation of 0.51 °C (Figure 4). The system consistently operated within a narrow band around the nominal setpoint, demonstrating precise control and high thermal stability.

After 123 min, the heating system was manually switched off to evaluate the performance of the incubator's passive insulation (Figure 4). The subsequent cooling curve was fitted using a first-order exponential decay model:

$$T(t) = T_0 e^{-k(t-t_0)} + T_{ambient},$$

where *T(t)* is the internal temperature at time t, T_0 represents the initial temperature difference between the incubator and the environment ($T_{start} - T_{ambient}$), k is the cooling rate constant [1/min], $T_{ambient}$ denotes the ambient temperature, and t_0 marks the time of heating system deactivation.

The fitted parameters were $T_0 = 31.68$ °C, $k = 0.062$ min^{-1}, and $T_{ambient} \approx 0.09$ °C. While the actual ambient temperature was –5 °C, the fitted $T_{ambient}$ represents the asymptotic temperature under insulated decay conditions, damped by the thermal inertia of the incubator. Following deactivation of the heating system, internal temperatures declined gradually, remaining above 32 °C for approximately 5 min. This passive thermal buffer suffices to bridge short power interruptions or final handling steps without immediate sample degradation. The observed performance confirms the functional contribution of the internal insulation in delaying heat loss after shutdown.

3.2. Battery-Powered Operation Under Cold Conditions

The second validation experiment investigated the incubator's performance under autonomous battery-powered operation in a realistic deployment scenario (Figure 5). Unlike standard laboratory procedures, where the system would ideally be preheated to the target temperature before sample loading, this test simulated a sudden and time-critical deployment—for example, in response to last-minute rocket readiness—where no time is available for preconditioning. The incubator, initially at room temperature, was transferred into a cold environment and operated under battery power alone to reach and maintain 37 °C, with the lid kept closed to simulate realistic transport conditions and minimize convective heat loss.

To replicate field conditions, the incubator was exposed to an ambient temperature of −5 °C and a wind speed of 0.5 m/s. Immediately after start of experiment, the battery-powered heating system was activated and temperature regulation started. Internal temperature was logged at 1min intervals using the internal Dallas temperature sensor.

The incubator reached the target temperature of 37 °C within 5 min. For the subsequent 76 min, it maintained a stable internal temperature with a mean of 37.55 °C and a standard deviation of 0.82 °C. The observed mean deviation lies within the defined requirement of maintaining ±1 °C accuracy around the setpoint and is considered biologically acceptable for short handling periods. The thermal control loop is deliberately tuned for robustness under cold deployment conditions, prioritizing rapid recovery. Importantly, during the initial warm-up phase, no biological samples or experimental hardware are present inside the incubator, so the brief overshoot during startup poses no risk to payload integrity. For highly heat-sensitive payloads, however, a conservative alternative (reduced P, increased I with anti-windup) can be selected to minimize overshoot and oscillation at the expense of a slower warm-up. The incubator was intentionally left empty for this test to isolate the thermal performance of the system itself. This configuration reflects typical deployment scenarios, in which experimental hardware—having been preheated in laboratory conditions—is already at or near target temperature upon integration. The slight positive deviation from the nominal setpoint reflects a conservative controller configuration, favoring thermal robustness and mission readiness under uncertain environmental conditions.

The incubator's battery voltage was continuously monitored at 1 Hz with an external voltmeter (Keithley DMM6500) to assess power demand during autonomous heating. The recorded voltage profile exhibited pronounced fluctuations, with values ranging from a maximum of 24.25 V to a minimum of 21.40 V, resulting in an overall fluctuation range of 2.85 V. These periodic voltage drops corresponded to the duty cycles of the heating system, reflecting the high instantaneous current draw during active heating phases. The near-digital appearance of the voltage trace results from this time-proportioning actuation:

the PI controller (D = 0) computes a continuous control signal that is translated into a duty cycle, producing discrete load steps visible as voltage plateaus.

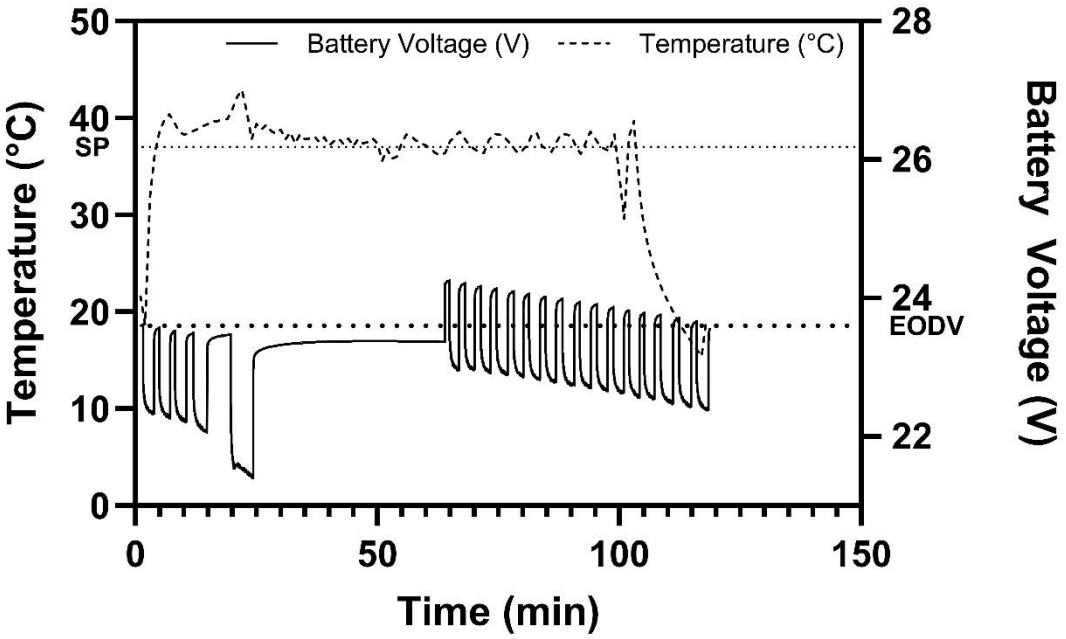

Figure 5. Internal temperature and battery voltage of the transport incubator over time during battery-powered operation at −5 °C ambient temperature and a wind speed of 0.5 m/s. The incubator reached and maintained the setpoint temperature (SP) of 37 °C for over 100 min. Battery voltage fluctuated periodically due to the heating system's duty cycling. After ~110 min, the voltage dropped below the end-of-discharge threshold (EODV), resulting in a gradual decline of internal temperature due to passive cooling.

While the nominal end-of-discharge voltage (EODV) was defined at 23.6 V, measured voltage values temporarily dipped below this threshold early in the experiment. This behavior is consistent with brief high-load periods rather than sustained discharge, as the system continued to operate reliably and maintain thermal regulation for over 100 min. These transient under-voltages are characteristic of pulsed high-power loads in battery-operated systems and do not indicate battery depletion at that time.

The voltage trend provides insight into the power dynamics of the heating system and highlights the interplay between temperature control precision and energy availability. While the thermal system itself exhibits significant inertia and is not directly affected by high-frequency fluctuations, the observed voltage dips correspond to discrete heating cycles with elevated current draw. The control architecture manages these transient power demands without compromising thermal regulation. Moreover, the distinct drop-off in temperature observed later in the experiment aligns with the expected onset of sustained undervoltage conditions, suggesting that the battery reached its functional discharge limit (t = 100 min).

In summary, this experiment validated the incubator's ability to achieve and maintain its target temperature using internal battery power alone for over 100 min under adverse thermal conditions. The results also highlight the thermal buffering capacity of the system: once active heating ceases due to battery depletion; the internal temperature decreases only gradually. This demonstrates that the passive insulation effectively prolongs thermal protection beyond the limits of active regulation, ensuring a continued safeguard for biological samples during power loss scenarios.

3.3. Thermal Modeling and Simulation

While experimental validation is essential for verifying system performance, the test scenarios are primarily limited to the environmental conditions and provide only a limited number of different boundary conditions. To support extrapolation beyond the test scope, a numerical thermal model was developed based on the finite difference method (FDM). This model enables prediction of incubator behavior across a wide range of mission-relevant conditions, such as variable ambient temperatures, airflow rates, degraded insulation, and system-level design variations.

The thermal model supports virtual stress testing under boundary conditions that are difficult or costly to realize physically and covers situations that can occur in mission-critical scenarios, such as high wind exposure, extended power outages, or altered convection paths. It also provides insight into local temperature gradients, internal heat flows, and worst-case heating power requirements that are important for battery sizing, control strategy development, and system scaling.

3.3.1. Model Structure and Boundary Conditions

The incubator was modeled using a steady-state FDM approach. It was discretized into 14 thermal nodes representing different structural and internal segments (Figure 6). The incubator was modeled as an aluminium box with a wall thickness of 0.8 mm, covered in 19 mm insulation with a thermal conductivity of λ = 0.033 W/(m·K). Insulation was modeled for all walls, except the left-hand side, where the electronic components are attached, without additional insulation. Conductive heat transfer between adjacent nodes was described by

$$G_{L\ a\to b} = \frac{\lambda\, A}{L} \quad \left[\frac{W}{K}\right]$$

where λ is the thermal conductivity, L is the distance between nodes, A is the effective area, and G_L is the conductance between adjacent nodes a and b.

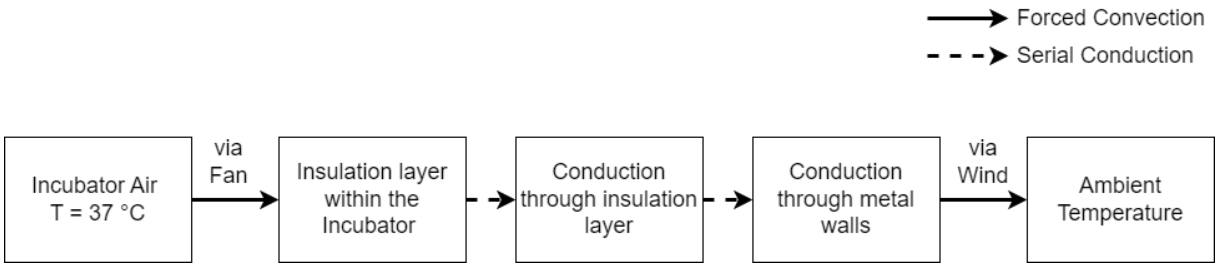

Figure 6. Thermal model structure and boundary condition assumptions used in the finite difference simulation. Insulation was modeled for all internal walls, except for the left-hand side, where the electrical components are attached and which is therefore not insulated. All outer surfaces are subjected to forced convection except the bottom face.

Convective heat exchange was implemented in accordance with VDI guideline 2056 using the Gnielinski correlation [27]. Forced convection was applied to all external surfaces except the bottom face, which was considered insulated. This assumption reflects the experimental validation setup, where the incubator was placed directly on the ground. Contact was minimized by a metal frame that lifts the bottom about 10 mm, resulting in limited convective and conductive coupling to the surface. Internally, forced convection was applied uniformly across all surfaces, driven by the integrated circulation fans. Radiative exchange and humidity effects were neglected in the current implementation. The system was solved under steady-state conditions. A conductance matrix G_L was assembled according to the nodal configuration illustrated in Figure 7, leading to the following linear formulation:

$$G_L \vec{T} + \vec{q} = \vec{0},$$

where $\vec{T}$ represents the nodal temperature vector and $\vec{q}$ shows the internal and external heat flows. The incubator target temperature was fixed at 37 °C, representing the maximum internal target temperature and thereby the worst-case thermal load condition. Ambient temperature and convective heat transfer coefficients were varied parametrically to represent different mission environments.

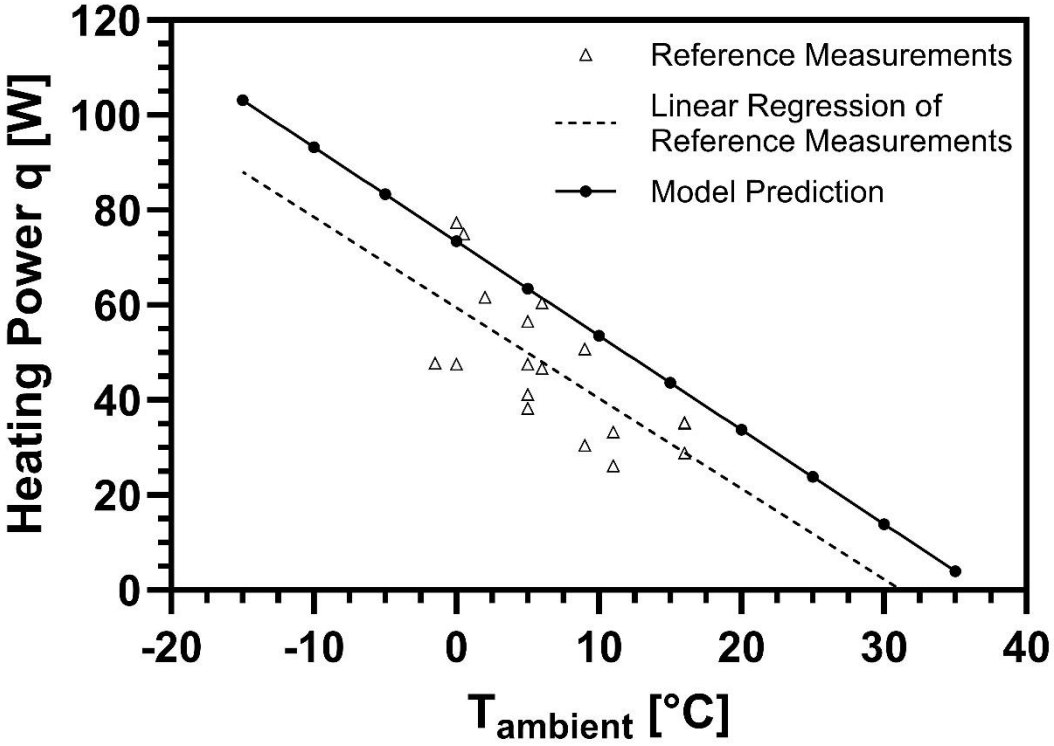

Figure 7. Required heating power as a function of ambient temperature for the transport incubator at a fixed internal target temperature of 37 °C. The model prediction (solid line) is based on a steady-state finite difference model with 14 thermal nodes, accounting for conduction, forced convection, and passive insulation. Experimental reference measurements (triangles) were performed at ambient temperatures between 0 °C and 15 °C. The dashed line shows the linear regression of all reference data. The model demonstrates good agreement with worst case measurements, suitable for future mission planning in regard to maximal power loads needed for varying ambient conditions.

3.3.2. Experimental Validation and Results

A set of twelve model permutations were generated and compared based on a series of reference measurements, conducted at ambient temperatures between 0 °C and 15 °C. Each model includes a fixed set of boundary conditions, for instance constant wind and fan speeds, which result in a linear heating power demand over different ambient temperatures. Conduction through the insulation layer forms the dominant thermal pathway between the interior and exterior. The magnitude of this heat flow is sustained by convective cooling at the incubator's outer shell, which continuously enforces an energy loss, resulting in a temperature difference between inside and outside. This, in turn, increases the power loss via conduction, which is dependent on this difference. Radiative exchange was neglected. The bottom surface was modeled as insulated, reflecting the slightly elevated installation of the incubator and negligible convective coupling at the bottom. Direct conductive exchange would only occur if the unit were placed in soft snow; in that case, initial melting would limit sustained contact. This boundary condition was therefore neglected as a

minor influence compared to convective losses at the outer shell. All simulations were implemented in MATLAB R2022a using the standard ODE solver suite (ODEbox Version 1.1, Solver ode45)

To improve robustness, a total of 18 measurements with varying ambient conditions were conducted and used for benchmarking. An anemometer was used to quantify the wind speed. Factors leading to altered waste heat like varying solar radiation, cloud coverage and changes in relative humidity were not quantified. The incubator's electrical power consumption was recorded at thermal steady state. For this purpose, the incubator was pre-heated in the laboratory to the target temperature of 37 °C, before being placed outside and switched to battery operation. Since the model computes only the heating power necessary to maintain the target temperature, a baseline power consumption of 17.30 W at room temperature (standard deviation: 2.03 W)—representing all electrical loads excluding heaters—was experimentally determined and subtracted from the total power draw. This baseline arises predominantly from conversion electronics located outside the incubator's conditioned volume; only a negligible fraction couples thermally back into the interior. Accordingly, it was treated as an external load rather than as an internal heating contribution. As the thermal model shall assist in mission planning by predicting worst case power requirements, the model permutations were traded against the maximal power consumption measured. In low temperature verification scenarios, deviations of up to 40% were observed in power consumption measurements. The model variant with best agreement of the worst-case power loads was chosen as prediction tool for future missions. It assumed forced convection on all exposed surfaces and incorporated the internal passive insulation used in the actual hardware.

The required heating power as a function of ambient temperature was captured with

$$q\,(T) = -1.9837\,T_{ambient} + 73.398$$

This implies a heating power increase of approximately 10 W per 5 °C drop in ambient temperature. The effective G_L equals 1.984 W/K (model-wise). At 0 °C, the reference measurement yields G_L = 2.091 W/K—a deviation of 5.12%. At 15 °C, the reference measurement yields G_L = 1.633 W/K—a deviation of 21.49%. As can be seen in Figure 7, the worst-case model predictions reliably yielded higher power requirements than actually needed in the tests. Only at 0 °C, model predictions were lower than measured (5.12%). As expected, fluctuation in the required heating output continues to increase as the difference between the target temperature and ambient temperatures increases. For the mission application we therefore suggest a safety factor of 1.2–1.3. We hereby provide a conservative model for limits in in-field deployment (Figure 7).

4. Discussion and Outlook

The development and successful operation of the transport incubator represent an advancement in the form of a validated, technically enabling platform in the available infrastructure for biological research in extreme environments. Traditional transport systems, typically relying on passive insulation, lack the active control, responsiveness, and autonomy required for current and future space applications. The incubator addresses this technological gap by combining active thermal regulation, adaptable power management, and mechanical protection in a compact, field-deployable platform.

Its capabilities were diversely validated through field missions, thermal modeling and controlled experiments. During three MAPHEUS sounding rocket campaigns, the system reliably maintained physiological conditions for different biological payloads—including sensitive primary neuronal cultures and multicellular organisms—under sub-zero ambient temperatures, deep snow, and turbulent helicopter-based recovery logistics. These missions

confirmed the incubator's readiness for real-world use and its potential to safeguard sample integrity under dynamic and thermally challenging conditions. Complementary to these operations, two ground-based experiments provided insight into the system's thermal behavior under controlled cold stress. In the first experiment, the incubator demonstrated an exponential heating response, reaching thermal equilibrium at 42 °C after environmental pre-cooling to –5 °C. Once stabilized, it maintained a narrow temperature band (mean: 37.81 °C, SD: 0.51 °C) for over 35 min, followed by an exponential cooling phase after manual shutdown. The experiment validated not only the efficiency of the heating system, but also the function of the passive insulation in preserving thermal conditions during power loss (Figure 4).

In the second experiment, the incubator was tested in a battery-only cold-start scenario without preheating. The system reached 37 °C within 5 min, then maintained that level for 76 min with low deviation (mean: 37.55 °C, SD: 0.82 °C), demonstrating the feasibility of rapid deployment without infrastructure. Real-time battery monitoring revealed cyclic voltage drops associated with heating load. The system operated up to the effective end-of-discharge threshold. The experiment confirmed autonomous performance, tolerance to high load dynamics, and fall back to passive thermal protection upon power exhaustion (Figure 5).

The overshoot observed during the initial heating phase results from the controller's intentionally aggressive configuration. The PI algorithm was tuned with a strong proportional component to ensure rapid thermal response—particularly relevant when transitioning from warm laboratory environments to sub-zero field conditions. This tuning leads to a control behavior that, in its initial phase, resembles that of a two-point controller, producing a steep rise in temperature until the setpoint is exceeded. The system is designed to tolerate this overshoot, as it allows for significantly faster mission readiness. In real-world campaigns, excess heat can be easily dissipated by briefly opening the incubator lid, whereas an overly conservative controller configuration would require prolonged heating durations—an unacceptable condition under tight operational constraints often encountered during rocket launches.

In addition to these empirical tests, a steady-state thermal model was developed to simulate heat flow and required power levels across a broader range of possible mission conditions (Figure 6). The model discretizes the incubator into 14 thermal nodes and calculates temperature distributions and thermal loads under defined boundary conditions. It was experimentally validated across 21 conditions between 0 °C and 15 °C, showing excellent agreement with measurement data (standard deviation to regression fit: 1.93 W). The derived regression predicts an increase in heating power of approximately 10 W per 5 °C drop in ambient temperature, thus enabling robust mission planning beyond the experimentally proven range.

Importantly, the model was deliberately limited to steady-state conditions. For short-term use, thermally buffered transport phases with quasi-stationary outer conditions, a dynamic model would introduce significantly more complexity. The computational simplicity and speed of the current model allow efficient evaluation of worst-case scenarios and design variants (e.g., insulation concepts, surface modifications) during early planning phases. For time-dynamic missions or transiently shifting thermal boundaries, model extensions could include time-dependent heat flow, inhomogeneous material properties, and radiative exchange.

Besides the successful operation and validation of the transport incubator, several limitations remain that may be addressed in future iterations of the system.

The current PI temperature control algorithm is tuned for rapid convergence under cold-start conditions, prioritizing fast thermal response in sub-zero environments. While effective for arctic deployment scenarios, this configuration leads to a moderate overshoot

during initial heating. The discrete step-like appearance of the battery voltage observed in the field tests is characteristic of the time-proportioning actuation of the heaters and does not impair thermal regulation. A more adaptive PI tuning, possibly incorporating ambient feedback or load estimation, could improve regulation precision under varying environmental conditions.

Furthermore, initial tests suggest that under elevated ambient temperatures exceeding ~30 °C, the internal thermal load from the onboard power supply's own electrical dissipation may impair the ability to maintain low or physiological setpoints. In such cases, passive heat rejection alone may be insufficient to prevent unintended internal temperature rise. Future versions of the incubator could include an additional thermostatically controlled exhaust fan, enabling active heat extraction from the electronics compartment during warm weather operation or extended standby periods.

In scenarios involving stronger mechanical loading or pronounced lateral movement—such as during long-distance overland transport—custom-fitted internal mounting frames could be developed to provide experiment-specific mechanical stabilization. In addition, the integration of polymer foam layers could be considered for future versions to combine insulation with enhanced damping properties, thereby tailoring the incubator to more demanding transport profiles without compromising its modularity or biological compatibility.

Additionally, a systematic mapping of spatial temperature homogeneity was beyond the scope of this work and will be addressed in future iterations. A dedicated acoustic over-temperature alarm could further support field operation with heat-sensitive payloads.

These refinements would further expand the operational temperature range and enhance system stability under less favorable boundary conditions, reinforcing the incubator's robustness for diverse mission profiles and transport environments.

Viewed in concert, these results confirm that our transport incubator enables high-precision thermal control, not only under idealized conditions but also under severe real-world constraints. Its integrated laboratory power supply further allows pre-launch sample monitoring and physiological readouts until final integration—adding a new dimension of control and reproducibility to suborbital biological research. The reliability and practical relevance of these capabilities have been demonstrated across field and laboratory settings, leading to the submission of a patent application to the German Patent Office (Application No. 10 2024 135 428.3).

Beyond its validated architecture, the incubator's modular system design enables future expansion and customization, establishing it as a flexible enabling platform for mission-specific extensions and the integration of new payload types. Possible enhancements include CO_2 level or pressure control for advanced biological applications, miniaturization of control electronics to reduce mass, and improved battery management for extended missions. The addition of an internal data logger with acceleration sensing and environmental telemetry would support unattended long-distance operation, such as truck transport powered via vehicle voltage supply.

For orbital missions and ground segment logistics, the system could serve as an intermediary transport layer for Standard or Advanced Experiment Containers (SEC/AEC), as well as sealed payloads requiring triple containment (ECDS) [28,29]. This would facilitate precise environmental control during handover phases between laboratories, integration facilities, and launch pads.

In synthesis, the transport incubator offers a robustly validated and highly adaptable platform for the safe transport of biological payloads under extreme environmental conditions. It combines robust field performance with precise thermal control and simulation-

supported design, positioning it as a cornerstone infrastructure for modern gravitational biological research on Earth, in orbit, and beyond.

5. Patents

A patent application covering the described transport incubator has been submitted to the German Patent Office (Application No. 10 2024 135 428.3). A European patent and international protection (including for the U.S.) are currently being pursued.

Author Contributions: Conceptualization, S.F.; methodology, S.F. and I.M.H.; software, S.F.; validation, S.F. and I.M.H.; formal analysis, S.F. and I.M.H.; investigation, S.F. and I.M.H.; resources, J.H.; data curation, S.F. and I.M.H.; writing—original draft preparation, S.F. and I.M.H.; writing—review and editing, S.F., I.M.H. and J.H.; visualization, S.F.; supervision, J.H.; project administration, S.F. and J.H.; funding acquisition, J.H. All authors have read and agreed to the published version of the manuscript.

Funding: This research received no external funding.

Data Availability Statement: The data that support the findings of this study are available from the corresponding author upon reasonable request.

Acknowledgments: We would like to thank the MAPHEUS team of the Institute for Frontier Materials on Earth and in Space at the German Aerospace Center (DLR) in Cologne for the opportunity to be part of the MAPHEUS sounding rocket project. The authors gratefully acknowledge colleagues from the Biology Department for their early conceptual considerations and helpful discussions on defining operational requirements for biological sample handling during pre-launch and launch phases. We also acknowledge the support of DLR Mobile Rocket Base (MORABA) and Swedish Space Corporation (SSC) for on-site as well as overall support at ESRANGE Space Center during the campaigns. All individuals included in this section have consented to the acknowledgement.

Conflicts of Interest: The authors declare no conflicts of interest.

Abbreviations

The following abbreviations are used in this manuscript:

1U/2U	Standardized unit sizes for payload modules (1U = $10 \times 10 \times 10$ cm ^{3})
°C	Degrees Celsius
AEC	Advanced Experiment Container
ATMega2560	Microcontroller by Atmel (used in Arduino-compatible systems)
CO_2	Carbon Dioxide
DLR	German Aerospace Center (Deutsches Zentrum für Luft- und Raumfahrt)
ECDS	Experiment Container Double Sealed
EODV	End of Discharge Voltage
ESRANGE	European Space and Sounding Rocket Range
ESD	Electrostatic Discharge
FDM	Finite Difference Method
MAPHEUS	Materialphysikalische Experimente unter Schwerelosigkeit
m^3/h	Cubic meters per hour (airflow rate)
NBR	Nitrile Butadiene Rubber
PI	Proportional-Integral (controller)
PTC	Positive Temperature Coefficient
SD	Standard Deviation
SEC	Standard Experiment Container
SP	Setpoint
SSC	Swedish Space Corporation
W/(m·K)	Watt per meter-Kelvin (thermal conductivity)

References

1. Ferranti, F.M.; Del Bianco, M.; Pacelli, C. Advantages and Limitations of Current Microgravity Platforms for Space Biology Research. *Appl. Sci.* **2021**, *11*, 68. [CrossRef]
2. Ruyters, G.M.; Braun, M.; Stang, K.M. Space Life Sciences in the Exploration Era: An Outlook on Future Challenges and Opportunities. In *Breakthroughs in Space Life Science Research: From Apollo 16 to the ISS*; Springer International Publishing: Cham, Switzerland, 2021; pp. 139–155.
3. Abrahamsson, M.; Florin, G.; Lockowandt, C. Esrange Space Center—A European Rocket and Balloon Launch and Operation Site North of the Arctic Circle. In Proceedings of the 2018 SpaceOps Conference, Marseille, France, 28 May–1 June 2018.
4. Thrane, E.V. The history of Andøya Rocket Range. *Hist. Geo-Space Sci.* **2018**, *9*, 141–156. [CrossRef]
5. Fischer, K.; Kölzow, N.; Höltje, H.; Karl, I. Assay conditions in laboratory experiments: Is the use of constant rather than fluctuating temperatures justified when investigating temperature-induced plasticity? *Oecologia* **2011**, *166*, 23–33. [CrossRef] [PubMed]
6. Moradian, M.; Patnaik, A.; Han, Y.; Wan, F. Determination of the effect of humidity on the probability of ESD failure or upset in data centers. *ASHRAE Trans.* **2014**, *120*, 25–41.
7. Arnaud, O.; Meyer, S.; Vallin, E.; Beslon, G.; Gandrillon, O. Temperature-induced variation in gene expression burst size in metazoan cells. *BMC Mol. Biol.* **2015**, *16*, 20. [CrossRef]
8. Klein, S.G.; Steckbauer, A.; Alsolami, S.M.; Arossa, S.; Parry, A.J.; Li, M.; Duarte, C.M. Toward Best Practices for Controlling Mammalian Cell Culture Environments. *Front. Cell Dev. Biol.* **2022**, *10*, 788808. [CrossRef]
9. Feles, S.; Overath, C.; Reichardt, S.; Diegeler, S.; Schmitz, C.; Kronenberg, J.; Baumstark-Khan, C.; Hemmersbach, R.; Hellweg, C.E.; Liemersdorf, C. Streamlining Culture Conditions for the Neuroblastoma Cell Line SH-SY5Y: A Prerequisite for Functional Studies. *Methods Protoc.* **2022**, *5*, 58. [CrossRef]
10. Lichterfeld, Y.; Kalinski, L.; Schunk, S.; Schmakeit, T.; Feles, S.; Frett, T.; Herrmann, H.; Hemmersbach, R.; Liemersdorf, C. Hypergravity Attenuates Reactivity in Primary Murine Astrocytes. *Biomedicines* **2022**, *10*, 1966. [CrossRef]
11. Chishti, A.A.; Hellweg, C.E.; Berger, T.; Baumstark-Khan, C.; Feles, S.; Kätzel, T.; Reitz, G. Constitutive expression of tdTomato protein as a cytotoxicity and proliferation marker for space radiation biology. *Life Sci. Space Res.* **2015**, *4*, 35–45. [CrossRef]
12. Lee, W.; Moon, M.; Kim, H.G.; Lee, T.H.; Oh, M.S. Heat stress-induced memory impairment is associated with neuroinflammation in mice. *J. Neuroinflamm.* **2015**, *12*, 102. [CrossRef]
13. Kim, J.; Connors, B. High temperatures alter physiological properties of pyramidal cells and inhibitory interneurons in hippocampus. *Front. Cell. Neurosci.* **2012**, *6*, 25084. [CrossRef]
14. Kopchenko, P.V.; Rozovskii, A.S.; Saidal', G.I.; Smirnov, V.M. Use of the Synthetic Rubber Armaflex AC as Cryoinsulation. *Chem. Pet. Eng.* **2003**, *39*, 142–146. [CrossRef]
15. Blake, D.F.; Crowe, M.; Mitchell, S.J.; Aitken, P.; Pollock, N.W. Vibration and bubbles: A systematic review of the effects of helicopter retrieval on injured divers. *Diving Hyperb. Med.* **2018**, *48*, 235–240. [CrossRef] [PubMed]
16. Park, J.; Choi, S.; Jung, H.M. Measurement and Analysis of Vibration Levels for Truck Transport Environment in Korea. *Appl. Sci.* **2020**, *10*, 6754. [CrossRef]
17. Grosman-Dziewiszek, P.; Wiatrak, B.; Dziewiszek, W.; Jawień, P.; Mydlikowski, R.; Bolejko, R.; Szandruk-Bender, M.; Karuga-Kuźniewska, E.; Szeląg, A. Influence of 40 Hz and 100 Hz vibration on SH-SY5Y cells growth and differentiation—A preliminary study. *Molecules* **2022**, *27*, 3337. [CrossRef]
18. Steppe, L.; Liedert, A.; Ignatius, A.; Haffner-Luntzer, M. Influence of low-magnitude high-frequency vibration on bone cells and bone regeneration. *Front. Bioeng. Biotechnol.* **2020**, *8*, 595139. [CrossRef] [PubMed]
19. Lakatos, Á.; Kalmár, F.; Csáky, I. Material selection in order to minimize the heat loss of piping based on measurements and calculations. *AIP Conf. Proc.* **2019**, *2186*, 070011.
20. Weatherspark. Climate Data for Kiruna, Sweden. 2025. Available online: https://weatherspark.com/m/86559/12/Average-Weather-in-December-in-Kiruna-Sweden#Figures-Humidity (accessed on 7 November 2024).
21. May, G.J.; Davidson, A.; Monahov, B. Lead batteries for utility energy storage: A review. *J. Energy Storage* **2018**, *15*, 145–157. [CrossRef]
22. Prasad, G.K.; Rahn, C.D. Model based identification of aging parameters in lithium ion batteries. *J. Power Sources* **2013**, *232*, 79–85. [CrossRef]
23. Prasad, U.; Prakash, J.; Kannan, A.N.M.; Kamavaram, V.; Arumugam, G.K. Failure analysis of lead-acid batteries at extreme operating temperatures. *Battery Energy* **2023**, *2*, 20230008. [CrossRef]
24. Kargl, F. Science on MAPHEUS. In Proceedings of the RB-Institutsseminar Herbst 2018, Erlangen, Germany, 14 December 2018.
25. Striebel, J.; Kalinski, L.; Sturm, M.; Drouvé, N.; Peters, S.; Lichterfeld, Y.; Habibey, R.; Hauslage, J.; El Sheikh, S.; Busskamp, V.; et al. Human neural network activity reacts to gravity changes in vitro. *Front. Neurosci.* **2023**, *17*, 1085282. [CrossRef]
26. Feles, S.; Keßler, R.; Hauslage, J. Pioneering the Future of Experimental Space Hardware: MiniFix-a Fully 3D-Printed and Highly Adaptable System for Biological Fixation in Space. *Microgravity Sci. Technol.* **2025**, *37*, 22. [CrossRef]

27. Grulich, M.; Hildebrand, K.; Dürrmann, C.; Wever, P.; de Vera, J.P.P. Biological Experiments in BIOLAB Facility on board Columbus. In Proceedings of the International Astronautical Congress, IAC, Paris, France, 18–22 September 2022.
28. Hellweg, C.E.; Dilruba, S.; Adrian, A.; Feles, S.; Schmitz, C.; Berger, T.; Przybyla, B.; Briganti, L.; Franz, M.; Segerer, J.; et al. Space experiment "Cellular Responses to Radiation in Space (CellRad)": Hardware and biological system tests. *Life Sci. Space Res.* **2015**, *7*, 73–89. [CrossRef] [PubMed]
29. Maas, N.; de Vera, J.-P.; Schmidt, M.J.; Reimann, P.; Randall, J.G.; Feles, S.; Hemmersbach, R.; Schierwater, B.; Hauslage, J. apex Mk. 2/Mk. 3: Secure Live Transmission of the First Flight of Trichoplax adhaerens in Space Based on Components Off-the-Shelf. *Eng* **2025**, *6*, 241. [CrossRef]